

Suppressed fusion cross section for neutron halo nuclei

M. Ito

Institute of Physics, University of Tsukuba, Tsukuba 305-8571, Japan

K. Yabana, T. Nakatsukasa

*Institute of Physics and Center for Computational Sciences,
University of Tsukuba, Tsukuba 305-8571, Japan*

M. Ueda

Akita National College of Technology, Akita 011-8511, Japan

(Dated: December 2, 2024)

Fusion reactions of neutron-halo nuclei are investigated theoretically with a three-body model. The time-dependent wave-packet method is used to solve the three-body Schrödinger equation. The halo neutron behaves as a spectator during the Coulomb dissociation process of the projectile. The fusion cross sections of $^{11}\text{Be} - ^{209}\text{Bi}$ and $^6\text{He} - ^{238}\text{U}$ are calculated and are compared with measurements. Our calculation indicates that the fusion cross section is slightly hindered by the presence of weakly bound neutrons.

PACS numbers: 25.60.Pj, 25.70.Mn, 24.10.-i

Keywords: NUCLEAR REACTION, $^{209}\text{Bi}(^{10}\text{Be}, X)$, $(^{11}\text{Be}, X)$, $^{238}\text{U}(^4\text{He}, X)$, $(^6\text{He}, X)$, Calculated fusion cross section, Three-body model, Time-dependent wave-packet method

Physics at the dripline is one of current subjects in nuclear physics. Adding neutrons to a nucleus as many as possible, we often find that some neutrons are bound very weakly. These neutrons form a spatially extended neutron cloud which is called the neutron halo. The halo nuclei have been attracting many researchers since its discovery in the secondary beam experiment [1]. The neutron-halo nucleus exhibits many properties different from normal nuclei. For instance, it violates the nuclear saturation of density and binding energy. Experimentally, these nuclei are mostly studied with reactions using the secondary beam.

Since the halo nuclei are weakly bound and easily break up, developments of the reaction theories capable of describing coupling to the continuum channels are required. For reactions in medium and high incident energies, the Glauber and the eikonal theories have been successful [2, 3, 4, 5]. In these theories, the wave function of the halo neutron in the projectile is frozen during the reaction. The success of the eikonal theories rests on the fact that the dynamics can be well separated into fast and slow motions. Namely, the relative motion of projectile and target is much faster than that of halo neutrons. There is, however, no such clear distinction in collisions at low energy. In spite of many experimental and theoretical efforts in the last decade, the reaction mechanism of halo nuclei at low incident energies is still an open question.

The fusion of halo nuclei shows an example of the controversial subjects. In early stages, a simple and intuitive theoretical argument has been proposed [11, 12]: The fusion probability was expected to be enhanced because of the spatially extended density of the halo neutron. A further enhancement was predicted by the coupling to soft

modes inherent to the halo structure. Breakup effects were predicted to be small, sustaining a large enhancement of fusion cross section especially at sub-barrier energies [12, 13]. These early studies utilized a specific reaction model. We have developed a time-dependent wave packet method for fully quantum calculations using a three-body model [14, 15, 16, 17, 18]. Our results have disagreed with the fusion enhancement. In fact, the calculation has even suggested a slight suppression of the fusion probability because of the presence of the halo neutron. However, recent coupled-channel calculations using a similar three-body model, again, indicate a substantial enhancement in the fusion probability at sub-barrier energies [19, 20].

Experimental results also show a rather confusing status. In early measurements, an enhancement of the fusion cross section at sub-barrier energies was reported for reactions using a two-neutron-halo nucleus ^6He [6, 7]. Recently, however, Ref. [8] have reported that the enhancement previously obtained in Ref. [7] is not due to the fusion but to the transfer-induced fission. In case of a one-neutron-halo nucleus, ^{11}Be , the experimental results did not present an evident conclusion either [9]. A recent comparison between ^{10}Be and ^{11}Be fusion cross sections suggests no enhancement for ^{11}Be [10]. Thus, we may say, at least, that the present experimental status indicates no evidence for a fusion enhancement of halo nuclei.

In this letter, we report calculations of the fusion cross sections in the three-body model. We previously reported fusion probabilities of halo nuclei mostly for the case of total angular momentum $J = 0$ which corresponds to the head-on collision [16, 17, 18]. We now include a full range of impact parameter, for $0 \leq J \leq 30$, then, for the first time, present results of fusion cross sections calculated

with the time-dependent wave-packet method. Calculations are performed for fusion cross sections of $^{11}\text{Be} - ^{209}\text{Bi}$ and $^6\text{He} - ^{238}\text{U}$. Results are compared with experimental data [8, 10].

In our three-body model, the projectile is described as a weakly bound two-body system of the core and the halo neutron(s). The projectile (P), which is composed of the core (C) plus neutron(s) (n), and the target (T) constitute the three-body model. For ^{11}Be , we assume a $^{10}\text{Be}+n$ structure in which the halo neutron occupies a $2s$ orbital in the projectile ground state. For ^6He , a di-neutron model of $\alpha+2n$ is assumed. The time-dependent Schrödinger equation for the three-body model is given as

$$i\hbar \frac{\partial}{\partial t} \Psi(\mathbf{R}, \mathbf{r}, t) = \left\{ -\frac{\hbar^2}{2\mu} \nabla_{\mathbf{R}}^2 - \frac{\hbar^2}{2m} \nabla_{\mathbf{r}}^2 + V_{nC}(r) + V_{CT}(R_{CT}) + V_{nT}(r_{nT}) \right\} \Psi(\mathbf{R}, \mathbf{r}, t), \quad (1)$$

where we denote the relative n - C coordinate as \mathbf{r} and the relative P - T coordinate as \mathbf{R} . The reduced masses of n - C and P - T motions are m and μ , respectively.

The Hamiltonian in Eq. (1) includes interaction potentials among constituents. The n - C potential, $V_{nC}(r)$, is a real potential. This potential should produce a halo structure of the projectile. The core-target potential, $V_{CT}(R_{CT})$, consists of the nuclear and Coulomb potentials. The nuclear potential is complex and its short-ranged imaginary part is inside the Coulomb barrier between the core and the target nuclei. The n - T potential, $V_{nT}(r_{nT})$, is taken to be real. We treat the constituents as spin-less point particles, and ignore the non-central forces. The nuclear potentials of V_{nC} , V_{CT} , and V_{nT} are taken to be of a Woods-Saxon shape. For $^{11}\text{Be} - ^{209}\text{Bi}$ reaction, we take $V_0 = -53$ MeV, $r_0 = 1.3$ fm, $a = 0.7$ fm for V_{nC} , $V_0 = -65$ MeV, $r_0 = 1.16$ fm, $a = 0.8$ fm for the real part of V_{CT} , $V_0 = -60$ MeV, $r_0 = 0.6$ fm, $a = 0.4$ fm for the imaginary part of V_{CT} , and $V_0 = -44.019$ MeV, $r_0 = 1.27$ fm, $a = 0.67$ fm for V_{nT} . For $^6\text{He} - ^{238}\text{U}$ reaction, we adopt $V_0 = -69.305$ MeV, $r_0 = 0.667$ fm, $a = 0.65$ fm (V_{nC}), $V_0 = -95$ MeV, $r_0 = 1.1101$ fm, $a = 0.5834$ fm (real V_{CT}), $V_0 = -10$ MeV, $r_0 = 0.6$ fm, $a = 0.7$ fm (imaginary V_{CT}), and $V_0 = -93.4$ MeV, $r_0 = 0.986$ fm, $a = 1.184$ fm (V_{nT}). The V_{nC} provides the $2s$ bound orbital at -0.6 MeV for ^{11}Be , and -0.97 MeV for ^6He , which are close to the experimental separation energies of one and two neutrons, respectively.

We define the fusion cross section in terms of the loss of flux because of the imaginary potential in V_{CT} . The use of the imaginary potential is approximately equivalent to the incoming boundary condition inside the barrier. Once the core and the target nuclei are in the range of the imaginary V_{CT} inside the Coulomb barrier, the total flux decreases by the absorption, no matter whether the neutron is captured by the target or not. Therefore, this includes not only complete but also incomplete fusions.

The wave-packet calculation is performed with the partial wave expansion. Here, we use the partial wave expansion in the body-fixed frame [21, 22]. Although this is equivalent to the one in the space-fixed frame, the body-fixed frame is computationally superior for states at finite total angular momentum, $J \neq 0$. In the body-fixed frame, the channels are specified by the projection of J on the body-fixed z -axis, Ω , and the magnitude of the relative angular momentum conjugate to the angle between \mathbf{r}_{nC} and \mathbf{R}_{PT} which we denote as l . The coupling between different Ω channels is present only for $\Delta\Omega = \pm 1$, given by the Coriolis term. This sparse coupling term makes computations much easier in the body-fixed channel. Another advantage in the body-fixed frame is a natural truncation scheme set by the maximum value of Ω .

We adopt the model space of the radial coordinates, $0 < R < 50$ fm and $0 < r < 60$ fm, and discretize them with steps $(\Delta R, \Delta r) = (0.2, 1.0)$ fm ($\Delta R, \Delta r$) = $(0.3, 0.6)$ fm for ^{11}Be and ^6He , respectively. The maximum n - C relative angular momentum is taken as $l_{\text{max}} = 70$ to obtain converged results. If the n - T potential, V_{nT} is switched off, one can use a much smaller cutoff, typically $l_{\text{max}} = 4$. The discrete-variable representation is used for the second differential operator [23]. The time evolution of the wave packet is calculated employing the fourth order Taylor expansion method.

The initial wave packet in the incident channel is a spatially localized Gaussian wave packet multiplied with an incoming wave for the P - T relative motion while the n - C wave function is a bound orbital corresponding to the halo structure. The average P - T distance of the wave packet is set as 22 fm and the average incident energy approximately equal to the barrier top energy. The time evolution is calculated until the wave packet consists only of outgoing waves and the average P - T distance reaches 30 fm.

A single wave packet solution contains information for a certain range of energy. We extract the fusion probability for a fixed incident energy by the energy projection procedure [15].

Since the ground state of ^{11}Be is known to be well described by a single neutron halo model, our calculation for ^{11}Be is expected to be realistic. On the other hand, a di-neutron model for ^6He may be too crude. In order to include two-neutron correlation, we need a three-body $\alpha + n + n$ treatment for ^6He . Then, this requires a four-body description for the reaction, which is beyond the present computational ability. We consider the present di-neutron treatment may provide a qualitative description for ^6He .

Now, let us show the calculated results. In Figs. 1 and 2, we show calculated fusion probabilities at the head-on collision ($J = 0$) as a function of the incident energy. In Fig. 1, the fusion probability of $^{11}\text{Be} - ^{209}\text{Bi}$ (solid curve) is compared with that of $^{10}\text{Be} - ^{209}\text{Bi}$ (dotted). The latter is a result of a simple two-body calculation with the

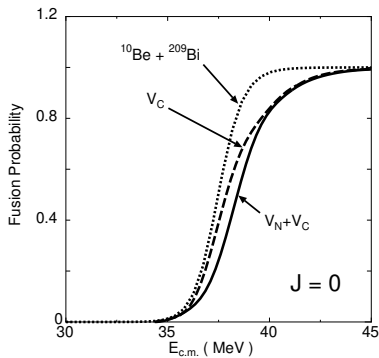


FIG. 1: Fusion probability of $^{11}\text{Be} - ^{209}\text{Bi}$ at $J = 0$. Calculation with V_{nT} (solid curve) is compared with that without V_{nT} potential (dashed), and two-body calculation without a halo neutron (dotted).

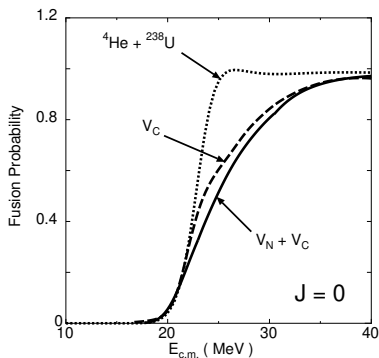


FIG. 2: The same as Fig. 1 but for $^6\text{He} - ^{238}\text{U}$.

V_{CT} potential. We also show, by a dashed line, a fusion probability of ^{11}Be calculated without the neutron-target potential, V_{nT} . Figure 1 indicates that the fusion probability is slightly suppressed by the presence of the halo neutron. The suppression is observed in both calculations with and without V_{nT} . This fact suggests that the suppression originates from the core-target Coulomb field which induces the dissociation of the halo neutron. The fusion probability of $^6\text{He} - ^{238}\text{U}$ system also shows a behavior similar to ^{11}Be (Fig. 2). The suppression of the fusion probability is seen to be even stronger than that of ^{11}Be . This may be due to a difference of the effective charges of the halo neutron: $(1/11)(4e)$ for ^{11}Be and $(2/6)(2e)$ for ^6He . The Coulomb dissociation effect is more significant for ^6He . There is only a minor difference between the solid and dashed curves for both cases, ^{11}Be and ^6He . We have confirmed that the results do not depend on choice of V_{nT} . Therefore, we conclude that reaction mechanism associated with V_{nT} does not play a major role in the fusion process of halo nuclei. It may be rather surprising that a long-ranged attractive potential of a halo nucleus, which is expected in a folding picture of V_{CT} and V_{nT} , does not contribute much to the fusion probability. This means that the reaction dynamics are

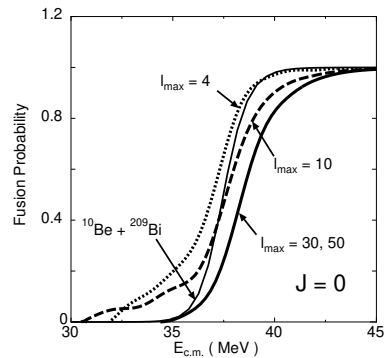


FIG. 3: Fusion probability of $^{11}\text{Be} - ^{209}\text{Bi}$ with different l_{max} . For reference, the fusion probability without a halo neutron is plotted by a thin-solid curve.

very different from those naturally expected by a simple picture.

In order to understand why, we should look in detail at the time evolution of the wave packet. Then, we find the following picture for the dynamics of halo nuclei [16]: When the core nucleus is decelerated by the target Coulomb field, the halo neutrons keep their incident velocity, leaving the core nucleus. This yields the Coulomb breakup of the projectile. After the breakup, the fusion takes place between two charged particles, the core and the target nuclei. The halo neutrons behave like a spectator. Based on this picture, we propose a mechanism that may explain the reason for the slight suppression of the fusion probability. The incident energy of the projectile is initially carried by the core and the halo neutron. After the Coulomb breakup, since the dissociated neutrons, as a spectator, keep their shared energy, the energy of the core nucleus is smaller than the total incident energy of the projectile. This practical decrease in the incident energy makes the fusion probability suppressed for a neutron-halo nucleus in comparison with the nucleus without halo neutrons. In this spectator picture, one may naively expect that effect of the breakup simply leads to an energy shift in curves of the fusion probability. However, our calculation indicates that the fusion probability above the barrier is suppressed, while the probability below the barrier is almost unchanged. Thus the effect is not that simple and depends on the incident energy.

In Refs.[19, 20], a strongly enhanced sub-barrier fusion probability was reported for halo nuclei by solving a similar three-body problem. This apparently disagrees with our results which indicate the suppressed fusion probability. We found that this discrepancy originates from a slow convergence of the calculated result with respect to l_{max} [16]. In the coupled-discretized continuum-channels (CDCC) approach which is adopted in Refs.[19, 20], a small value of l_{max} is applied for the n - C relative angular momentum, typically $l_{\text{max}} = 4$. In Fig. 3, we show

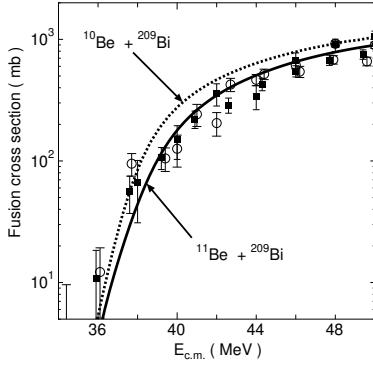


FIG. 4: Fusion cross section of $^{11}\text{Be} - ^{209}\text{Bi}$ (solid line) and $^{10}\text{Be} - ^{209}\text{Bi}$ (dotted line). Measured cross sections [10] are also shown: ^{11}Be by filled squares and ^{10}Be by open circles.

the fusion probability for different cutoff values of l_{max} . If we adopt a small l_{max} value, a strong enhancement of the sub-barrier fusion probability is obtained in our three-body calculations. This is consistent to results of the CDCC calculation [19, 20]. However, increasing l_{max} , the fusion probability gradually decreases, and eventually becomes smaller than the values without a halo neutron (dashed line). The result of $l_{\text{max}} = 30$ cannot be distinguished from that of $l_{\text{max}} = 50$. To get a converged result, therefore, one needs to adopt $l_{\text{max}} \geq 30$. We confirmed that this slow convergence with respect to l_{max} is due to the neutron-target potential, V_{nT} . If we ignore V_{nT} and includes only the Coulomb breakup induced by V_{CT} , the convergence is much faster, usually $l_{\text{max}} = 4$ is enough.

Extending the calculations to finite J up to $J = 30$, we achieve the total fusion cross section. In addition to l_{max} , we must also specify a maximum value of Ω which we denote as Ω_{max} . We compare fusion probabilities with $\Omega_{\text{max}} = 0, 5$, and 10 for a fixed J , and find that the results with $\Omega_{\text{max}} = 5$ and 10 are identical. Furthermore, a small difference between results of $\Omega_{\text{max}} = 0$ and $\Omega_{\text{max}} = 5$ is visible only for energies well above the barrier, $E > 42$ MeV. Thus, we here adopt the no-Coriolis approximation ($\Omega_{\text{max}} = 0$) to calculate the cross sections.

We show calculated fusion cross sections of $^{10,11}\text{Be} - ^{209}\text{Bi}$ in Fig. 4. The V_{CT} for $^{10}\text{Be} - ^{209}\text{Bi}$ is constructed so that the fusion cross section of this system is reproduced by a simple potential picture. Adding a halo neutron, the fusion cross section decreases slightly for an entire energy region. This is because the suppression of the fusion probability observed in the $J = 0$ also appears in finite J .

The measurement indicates that the fusion cross sections of ^{11}Be do not differ from those of ^{10}Be within the experimental error. At this stage, it is difficult to judge whether or not our calculated results of slight suppression in fusion cross section conflict with the measurements. In our calculation, a part of the halo neutron proceeds to

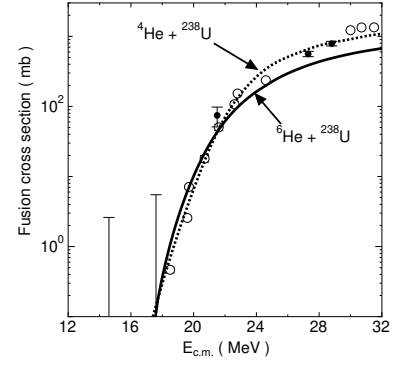


FIG. 5: The same as Fig. 4 but for $^6\text{He} - ^{238}\text{U}$. Experimental data are taken from Ref. [8], shown by open circles (^4He) and by filled circles (^6He). Two data points with large error bars at $E_{\text{c.m.}} \leq 18$ MeV indicate the data for ^6He .

the forward direction keeping the incident velocity after fusion. Therefore, the observation of these forward neutrons in the incomplete fusion process may support our picture. In Ref.[10], the forward neutron emission accompanying the fusion is discussed.

We next consider the fusion cross section of $^6\text{He} - ^{238}\text{U}$. In Fig. 5, we show the calculated fusion cross sections of ^6He and ^4He on ^{238}U . The experimental data in Ref.[8] indicate, again, that there is no difference between ^6He and ^4He fusion cross section within a statistical error. Our calculation indicates that the cross section for ^6He is suppressed from the one for ^4He at energies above the barrier. The magnitude of suppression in ^6He is larger than that in ^{11}Be at high energies. On the other hand, at sub-barrier energies, the calculated fusion cross sections of ^4He and ^6He are almost identical to each other. We again need to wait for measurements with high statistics to make a definite conclusion whether our calculation agrees with the experimental data.

In summary, we calculated the fusion cross section for nuclei with neutron halo structure. The reaction is described as the three-body model, and the three-body Schrödinger equation is solved exactly with the time-dependent wave-packet method. We compare calculated cross sections with measurements for $^{11,10}\text{Be} - ^{209}\text{Bi}$ and $^{6,4}\text{He} - ^{238}\text{U}$ collisions. Recent measurements of these systems suggest that there is no evidence for an enhancement in the fusion cross section of halo nuclei. Our calculation indicates that the fusion cross section is even suppressed by adding a halo neutron. Further measurements with increased statistics are desirable to obtain definite conclusion whether the fusion cross section is increased or suppressed by the presence of the halo neutron.

This work has been supported by the Grant-in-Aid for Scientific Research in Japan (Nos. 14540369 and 17540231). A part of the numerical calculations have been performed at RCNP, Osaka University and at SIPC, University of Tsukuba.

-
- [1] I. Tanihata et al., Phys. Rev. Lett. **55**, 2676 (1985).
 - [2] Y. Suzuki, R.G. Lovas, K. Yabana, and K. Varga, *Structure and Reactions of Light Exotic Nuclei*, Taylor and Francis, 2003.
 - [3] G.F. Bertsch, B.A. Brown, and H. Sagawa, Phys. Rev. **C39**, 1154 (1989).
 - [4] Y. Ogawa, K. Yabana, and Y. Suzuki, Nucl. Phys. **A543**, 722 (1992).
 - [5] K. Yabana, Y. Ogawa, and Y. Suzuki, Nucl. Phys. **A539**, 295 (1992); Phys. Rev. **C45**, 2909 (1992).
 - [6] J.J. Kolata et al., Phys. Rev. Lett. **81**, 4580 (1998).
 - [7] M. Trotta et al., Phys. Rev. Lett. **84**, 2342 (2000).
 - [8] R. Raabe et al., Nature **431**, (2004) 823.
 - [9] C. Signorini et al., Eur. Phys. J. A **2**, 227 (1998); **5**, 7 (1999).
 - [10] C. Signorini et al., Nucl. Phys. **A735**, 329 (2004).
 - [11] N. Takigawa and H. Sagawa, Phys. Lett. **B265**, 23 (1991).
 - [12] M.S. Hussein et al., Phys. Rev. **C46**, 377 (1992).
 - [13] N. Takigawa, M. Kuratani, and H. Sagawa, Phys. Rev. C **47**, R2470 (1993).
 - [14] K. Yabana and Y. Suzuki, Nucl. Phys. **A588**, 99c (1995).
 - [15] K. Yabana, Prog. Theor. Phys. **97**, 437 (1997).
 - [16] K. Yabana, M. Ueda, T. Nakatsukasa, Nucl. Phys. **A722**, 261c (2003).
 - [17] K. Yabana, M. Ito, M. Kobayashi, M. Ueda, and T. Nakatsukasa, Nucl. Phys. **A738**, 303 (2004).
 - [18] T. Nakatsukasa, K. Yabana, M. Ito, M. Kobayashi, M. Ueda, Prog. Theor. Phys. Suppl. **154**, 85 (2004).
 - [19] K. Hagino, A. Vitturi, C.H. Dasso, and S.M. Lenzi, Phys. Rev. **C61**, 037602 (2000).
 - [20] A. Diaz-Torres and I.J. Thompson, Phys. Rev. **C65**, 024606 (2002).
 - [21] T.T. Pack, J. Chem. Phys. **60**, 633 (1974).
 - [22] B. Imanishi and W. von Oertzen, Phys. Rep. **155**, (1987) 29.
 - [23] D.T. Colbert and W.H. Miller, J. Chem. Phys. **96**, 1982 (1992).